Fuzzy type two self-tuning technique of single neuron PID controller for brushless DC motor based on a COVID-19 optimization

Mohamed A. Abdel Ghany[1], Mohamed A. Shamseldin[2]
[1]Faculty of Engineering, October 6 University, Cairo, Egypt
[2]Faculty of Engineering and Technology, Future University in Egypt, Cairo, Egypt

Article Info

ABSTRACT

This paper presents an efficient interval type 2 fuzzy (IT2F) based on a single neuron proportional–integral–derivative (PID), also known as IT2FSNPID controller. The main purpose of the proposed control technique is to track the motion profile of the brushless DC (BLDC) motor. Also, a comparative study was investigated fuzzy type 1 (FT1) and IT2F. IT2F can treat the uncertainty and nonlinearity of the BLDC motor drive electric system in contrast to FT1. The parameters of each control technique were obtained using a new COVID-19 optimization algorithm according to an objective function. Moreover, several tests had been performed to ensure the ability of fuzzy type to absorb the system uncertainty and nonlinearity. All controllers were utilized to operate the BLDC motor sudden change in load and continuous load. The simulation results show that the IT2FSNPID can improve the dynamic response of linear and nonlinear of the same BLDC motor and accommodate the system uncertainty significantly.

Corresponding Author:

Mohamed A. Abdel Ghany
Faculty of Engineering and Technology, Future University in Egypt
S Teseen, New Cairo 1, Cairo Governorate 11835, Egypt
Email: mohamed.abelbbar@fue.edu.eg

1. INTRODUCTION

Often, the stator windings of the three-phase synchronous machine are operated by a DC source connected with a three-phase inverter which can called a brushless DC (BLDC) motor. The inverter's switching pulses are estimated by the rotor position. This position can be measured either by the hall effect sensor or by the sensorless technique. BLDC motor has many advantages compared to its DC counterpart [1], [2]. The BLDC motors have several advantages include long operating time, high dynamic performance, low losses, high range of speed–torque scale, and linear relationship between speed and torque of motor [3].

Because of these benefits, BLDC motors have been prioritized for use in a variety of applications, including robots, aviation, electric cars, and guided missiles [4]. The control strategy in such applications should force the rotor speed/position to track, independent of external disturbances, load, or parameter variations. To achieve this goal, the control approach used should be simple, reliable, and adaptable. In the face of parameter fluctuation, traditional control approaches cannot guarantee good performance [5]. The PID controller has a linear behavior with a simple design and great performance that is widely utilized. It's a great choice for a wide range of industrial applications [6], [7].

The selection of the proper PID parameters need to use an effective optimization technique to satisfy the required dynamic response. For this goal, several methods were proposed, including intelligent methods harmony search (HS), grey wolf optimization, dolphin optimization, firefly optimization, elephant

herding optimization, artificial bees optimization, whale optimization, cat optimization and COVID-19 optimization [8]-[12].

Another type of the PID controller can improve the performance is a single neuron PID (SNPID) controller. The single neuron (SN) controller features adaptive, self-learning, online tuning, and relatively reduced needs for controlled object stability and precision. Moreover, the SNPID controller has a simple and dependable construction [13]–[15]. The initial settings of the SNPID control gains can be found by trial and error at first, but this needs a long period of time. Now, most tuning optimization strategies (GA, PSO, flower pollination algorithm, harmony research (HS), an ant colony (ACO)) are based on computing a fitness function that represents the desired performance while satisfying system limitations. SNPID control performance is greatly influenced by the weights adjusting approach [16].

There are several learning algorithms for the weights of SNPID control according to the neural network (NN) learning theory which includes supervised delta learning rules, non-supervised Hebb learning rules, improved Hebb learning rule, and supervised Hebb learning rule [17]. The time of the weighs learning using the previous methods is high relative to new adaptive technique [18].

In this paper, a new COVID-19 optimization technique will be used to find the initial estimated of weights and learning rate factors. The fuzzy logic control system based on an expert knowledge database has a simple decision-making process and is well suited for modelling problems, either because the process is unknown or because it involves a large number of variable factors [19]–[24]. As a result, self-adaptive weights of the SNPID control can be achieved with self-tuning fuzzy logic control in this work to present an efficient method for accurately modifying the weights of SNPID control, resulting in a system that is more effective in disturbances. There are two types of fuzzy logic control approaches. The first approach is used fuzzy type 1 (FT1) which cannot deal with the system uncertainty while the second approach is interval type 2 fuzzy (IT2F) which treats the disadvantages of fuzzy type 1 (FT1). The high performance with fast dynamic response using an enhanced SNPID controller and an additional error of a converter control signal are presented in [25]. A single artificial intelligent neural network (NN) according to the PID control for intelligent sensors is demonstrated in [26]–[30].

The main purpose of this paper is design a interval type 2 fuzzy (IT2F) and compare it with FT1SNPID and SNPID controllers to ensure that the interval type 2 fuzzy (IT2F) can absorb the uncertainty and nonlinearity of the synchronies machine drive system which fed by an inverter. Also, a new COVID-19 optimization technique was developed to find the optimal parameters of each control technique. The remainder of this paper is organized as follows; part 2 shows the mathematical model of the BLDC motor drive system. The proposed control algorithms are demonstrated in part 3. Part 4 illustrates the discussion and simulation results. Recently, part 5 is the conclusion.

2.   MATHEMATICAL of BLDC MOTOR DRIVE SYSTEM

A synchronous motor employing a direct current (DC) electric power source is referred to as a brushless DC electric motor (BLDC motor or BL motor), sometimes known as an electronically commutated motor (ECM or EC motor), or synchronous DC motor. It uses an electronic controller to switch DC currents to the motor windings, creating magnetic fields that, when the permanent magnet rotor follows them, effectively rotate in space. To regulate the motor's speed and torque, the controller modifies the DC current pulses' phase and amplitude. The mechanical commutator (brushes) found in many conventional electric motors can be replaced by this control system.

A brushless motor system is often built similarly to a permanent magnet synchronous motor (PMSM), although it can also be an induction (asynchronous) motor or a switching reluctance motor. They could also be axial, out runners (the rotor is encircled by the stator), or in runners (the rotor is surrounded by the stator). Neodymium magnets might also be used (the rotor and stator are flat and parallel). High power-to-weight ratio, high speed, almost immediate control of speed (rpm) and torque, high efficiency, and cheap maintenance are all benefits of brushless motors over brushed motors. Brushless motors are used in a variety of devices, including hand-held power tools, model aero planes, automobiles, and computer peripherals (disc drives, printers). Brushless DC motors have made it possible for direct-drive designs to replace rubber belts and gearboxes in contemporary washing machines.

The behavior of the BLDC motor can be modelled into two techniques. The first technique simplifies the model to a linear model and neglects the nonlinearity and uncertain-ty resources such as the three-phase inverter and the three-hall effect sensor. The second technique takes into account the system's nonlinearity and uncertainty. Both two techniques will be considered. So, some of the tests will be performed on linear systems such as the parameters variation which is difficult to execute on the nonlinear model. The output transfer function of the BLDC motor drive system at no-load can be presented as follows [31].

Trapezoidal and sinusoidal BLDC motors are the two primary types. For ripple-free torque functioning in a trapezoidal motor, the phases of the back-emf induced in the stator windings must be supplied with quasi-square currents. The back-emf of a sinusoidal motor, on the other hand, has a sinusoidal shape and necessitates sinusoidal phase currents for torque operation without a ripple.

The arrangement of the stator windings and the design of the rotor magnets influence the back shape. Emf's The sinusoidal motor requires a high-resolution position sensor because, for optimal operation, the rotor location must be known at all times. Additionally, more complicated hardware and software are needed.

The simplicity, low cost, and improved efficiency of the trapezoidal motor make it a more appealing solution for the majority of industrial applications. This kind of motor also provides a good balance between the quantity of potent electronic components required to control the stator currents and precision control. This chapter's final section only covers the topic of trapezoidal BLDC motors.

$$G_u(S) = \frac{\omega(S)}{U_d(S)} = \frac{K_T}{L_a J S^2 + (r_a J + L_a B_v) S + (r_a B_v + K_e K_T)} \tag{1}$$

Where U_d is the DC source voltage, r_a is the line resistance of stator, L_a is the equivalent line inductance of stator, B_v is the viscous damping coefficient, J is the estimated rotor winding moment of inertia, ω is the instant rotor speed, K_e is the coefficient of phase back-EMF coefficient, and K_T is the constant of line phase torque. The construction of a BLDC motor drive electric system is illustrated in Figure 1 is a block diagram. Six-transistors voltage source inverters, a logic pulse circuit, and three hall effect sensors make up the master parts of the drive electric system.

The controller must be aware of the rotor's direction with respect to the stator coils in order to implement the functionality of the conventional brushes. Due to the fixed geometry of the rotor shaft and brushes, this occurs automatically in brushed motors. To directly measure the position of the rotor, some designs include Hall effect sensors or rotary encoders. Others determine the rotor position by measuring the back-EMF in the undriven coils, doing away with the necessity for separate Hall effect sensors. Thus, these are frequently referred to as sensorless controllers.

Because no back-EMF is generated when the rotor is stationary, controllers that detect rotor location based on back-EMF have additional difficulties in starting motion. Typically, to do this, rotation is started at an arbitrary phase, and if it turns out to be incorrect, rotation is skipped to the proper phase. The motor may briefly run backwards as a result, complicating the startup process even further. Other sensorless controllers can determine the rotor position by detecting the winding saturation brought on by the location of the magnets. The three polarity-reversible outputs on a typical controller are managed by a logic circuit. Simple controllers use comparators that are driven by orientation sensors to decide whether to advance the output phase. A microcontroller is used by more sophisticated controls to regulate motor speed, control acceleration, and optimize efficiency. Table 1 lists the BLDC electric drive system specifications.
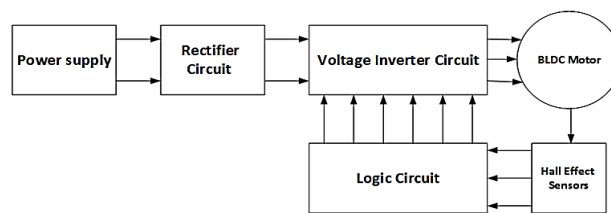

Figure 1. The BLDC motor drive electric system structure

Table 1. BLDC electric drive system specifications

Motor parameter	Terminology	Value	SI Units
Total resistance	R	0.57	Ω
Total Inductance	L	1.5	mH
Torque constant	K_T	0.082	N.m/A
No. of Poles	P	4	
Max. torque	T_p	0.42	N.m
Max. voltage	V	36	V
Rotor inertia	J	$23e^{-6}$	Kg.m^2
Determined friction coefficient	B_v	0.0000735	N.M.S
Max. speed	ω	4000	RPM
Max. current	I	5	A

Figure 2 illustrates the BLDC motor open loop response of machine drive system. The rotor speed of the motor accelerates to reach 4000 rpm in 0.05 seconds approximately. It is obvious that at time 0.25 seconds the unexpected load torque applied on the BLDC motor rotor which is estimated with 50% of Max. torque, the rotor winding speed falling from 4000 rpm to 3200 rpm. The matching BLDC electric drive phase current is shown in Figure 3. The initial current suddenly increases to 18 A in a short amount of time, whereas the phase current rises to 2.5 A due to the unpredicted load at time 0.25 seconds.

The BLDC motor consists of several nonlinear components such as the high-speed pulses inverter, Hall Effect sensor position sensor and bearing friction. These cause parameters uncertainty, sensitivity to disturbances and poor performance. The main objective of the proposed controller is absorbing the high nonlinearity from the motor drive system. There are two models executed to ensure the robustness of the proposed of control techniques. The first is a pure linear model and the second is a nonlinear and uncertainty model.
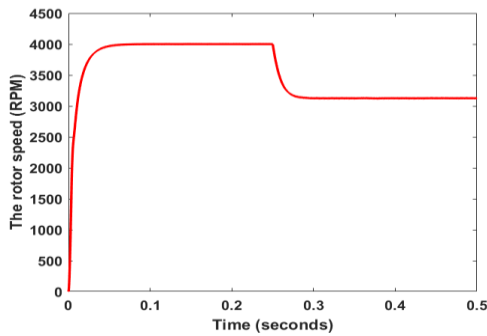

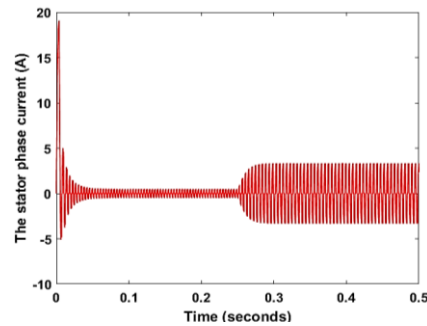Figure 2. The open system behavior of the BLDC drive system

Figure 3. BLDC motor model corresponding phase current

3. SNPID CONTROL TECHNIQUES

The main construction of three types of the proposed control techniques according to SNPID control is discussed in this section. The COVID-19 optimization method is used in the first control strategy to determine the best SNPID control parameters [32], while the second control technique uses the self-tuning fuzzy type 1 (STFT1) control to adapt the weights value of SNPID control. The third strategy is a novel hybrid control method that combines SNPID and fuzzy type 2 (FT2) control

3.1. Structure of SNPID controller

Single neuron PID (SNPID) considers the basic structure of neural network PIDs that beads on only one neuron. The equation of traditional PID in time domain is represented as (2).

$$u(t) = k_P\, e(t) + k_I \int_0^t e(t)dt + k_d \frac{de}{dt} \tag{2}$$

Where u(t) acts the output of controller and e is the controller error. The digitization can be implemented by differentiating both sides of (2) as (3).

$$u(t) = k_P\, e(t) + k_I\, e(t) + k_d \frac{de}{dt} \tag{3}$$

Using the backward diff. technique on (3) gives (4).

$$u(a) - u(a-1) = k_P\, [e(a) - e(a-1)] + k_I\, [\, e(a)] + k_d[\, \dot{e}(a) - \dot{e}(a-1)] \tag{4}$$

Applying the backward diff. method again for (4).

$$u(a) - u(a-1) = k_P[e(a) - e(a-1)] + k_I\, [e(a)]\, k_d[e(a) - e(a-1)] - [e(a-1) - e(a-2) \tag{5}$$

By calculation for u (a) finally from (5) gives the digital formula of the PID controller as (6).

$$u(a) = u(a-1) + k_P\, [e(a) - e(a-1)] + k_I\, [\, e(a)] + k_d[\, e(a) - 2e(a-1) + e(a-2)] \tag{6}$$

$$u(a) = u(a - 1) + k_P[x_1(a)] + k_I[x_2(a)] + k_d[x_3(a)] \tag{7}$$

$$x_1(a) = e(a) - e(a - 1)]$$
$$x_2(a) = e(a)$$
$$x_3(a) = e(a) - 2e(a - 1) + e(a - 2) \tag{8}$$

Where $x_1(a)$ is a proportional error, $x_2(a)$ is an integral error and $x_3(a)$ is a differential error. Figure 4 illustrates the construction of the SNPID controller.
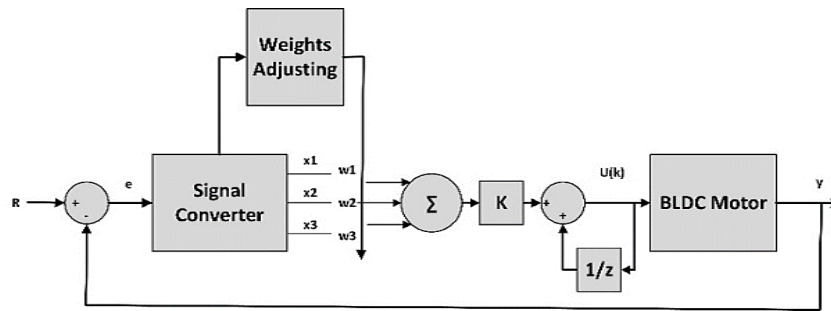

Figure 4. Main components of SNPID control

The SNPID controller can be expressed as (9) and (10).

$$u(a) = u(a - 1) + K \Sigma \overline{A}(a) x_i(a) \tag{9}$$

$$\overline{A}_i(a) = A_i(a) / \Sigma |A_i(a)| \tag{10}$$

The controller output and A_1, A_2 and A_3 are the neuron weights. Several weights learning techniques had been implemented according to the theory of neural networks. In this work the supervised Hebb learning rule was used. There are various weights learning algorithms based on the learning theory of neural networks and the famous algorithm that is used in this work is the supervised Hebb learning rule.

$$A_1(a) = A_1(a - 1) + \eta_p x_1(a - 1)u(a - 1)e(a - 1)$$
$$A_2(a) = A_2(a - 1) + \eta_i x_2(a - 1)u(a - 1)e(a - 1)$$
$$A_3(a) = A_3(a - 1) + \eta_d x_3(a - 1)u(a - 1)e(a - 1) \tag{11}$$

Where e is an error η_p, η_i and η_d are proportion learning speed, integral learning speed, and differential learning speed. there are several parameters that can be estimated by trial and error such as $A_1(a - 1), A_2(a - 1), A_3(a - 1), \eta_p, \eta_i, \eta_d$ and K but in this work, an efficient COVID-19 optimization technique will be used to investigate the proper values of these parameters.

3.2. The FT1SNPID controller

The fuzzy type 1 (FT1) was utilized to build self-tuning SNPID control to increase the robustness and flexibility of the SNPID controller. The learning rates are important criteria to consider when designing a SNPID control. To enhance the performance of the controller, the proportional, integral, and derivative learning rates are dynamically changed, and the weighted coefficients also vary in the same proportion. The fuzzy type 1 (FT1) is used to dynamically adjust the proportional, integral, and derivative learning rates. The self-tuning Type 1 SNPID controller structure is depicted in Figure 5.

According to in (12), the weights-learning algorithms used in this approach are supervised Hebb learning rules. The following describes how the learning rate is adjusted.

$$\eta_p(a) = \eta_p(a - 1) \times \Delta\eta_p(a)$$
$$\eta_i(a) = \eta_i(a - 1) \times \Delta\eta_i(a)$$
$$\eta_d(a) = \eta_d(a - 1) \times \Delta\eta_d(a) \tag{12}$$

Where $\Delta\eta_p$, $\Delta\eta_i$ and $\Delta\eta_d$ are the outputs of the fuzzy controller. Both error (e(t)) and delta error (Δe(t)) can be scaled from [-1,1]. Symmetric triangular fuzzy sets are used for the input and output variables, respectively, in the simulation in addition to the rule database of 49 fuzzy rules (shown in Figures 6 and 7). Tables 2, 3, and 4 simplify the rule bases. The linguistic labels for Fuzzy type 1 (FT1) are given as follows: N stands for negative; P is positive; Z represents zero; S is small; M is medium; and B is big. For example, NM stands for negative-medium, PB, for positive big, and so on. These 49 rule bases have been condensed into 25 rule bases for this paper, as stated in previous work in [21]. The details of the simplification can be found in [22].

There are several disadvantages of fuzzy ttype 1 in learning and updating the SNPID weights such as the poor performance through the system uncertainty and parameters variation [33]–[36]. So, to avoid these disadvantages the fuzzy type 2 will be applied instead of fuzzy type 1 as in the following section [37]–[42].
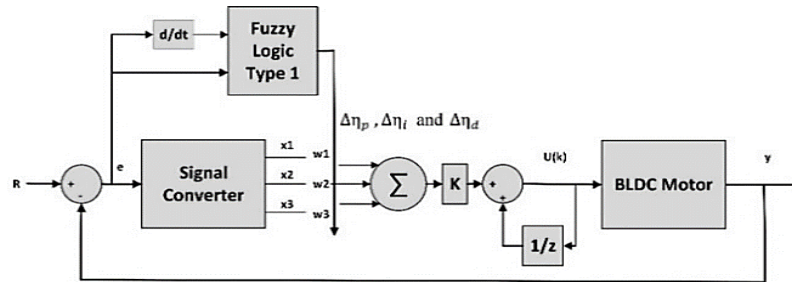
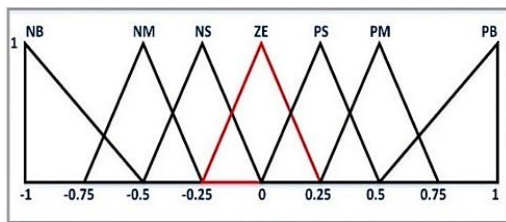

Figure 5. Controller block schematic for the FT1SNPID

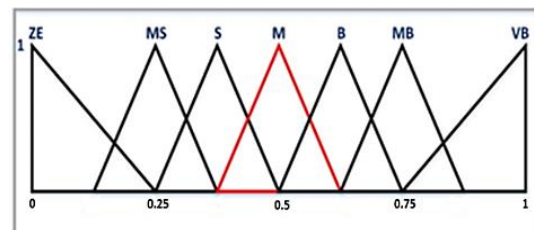Figure 6. Memberships function of inputs (error and delta error)

Figure 7. Memberships functions of outputs ($\Delta\eta_p$, $\Delta\eta_i$ and $\Delta\eta_d$)

Table 2. The Rule base of membership function of $\Delta\eta_p$

Δe/e	NB	NS	ZE	PS	PB
NB	ZE	S	M	MB	VB
NS	S	B	MB	VB	VB
ZE	M	MB	MB	VB	VB
PS	B	VB	VB	VB	VB
PB	VB	VB	VB	VB	VB

Table 3. The Rule base of membership function of $\Delta\eta_i$

Δe/e	NB	NS	ZE	PS	PB
NB	VB	VB	VB	VB	VB
NS	B	B	B	MB	VB
ZE	ZE	ZE	MS	S	S
PS	B	B	B	MB	VB
PB	VB	VB	VB	VB	VB

Table 4. The Rule base of membership function of $\Delta\eta_d$

Δe/e	NB	NS	ZE	PS	PB
NB	M	M	M	M	M
NS	S	S	S	S	S
ZE	MS	MS	ZE	MS	MS
PS	S	S	S	S	S
PB	M	M	M	M	M

3.3. The interval type 2 fuzzy SNPID controller

The properties of dynamic systems include typically inherent nonlinearities, uncertain parameters, and various disturbances. The control design is more challenging as the dynamic system gets more complicated, has more high-order nonlinearities, and has different kinds of uncertainties brought on by parameter changes and noise in the data. Therefore, one must manage their nonlinearities and uncertain parameters when regulating such dynamic systems.

Fuzzy type 1 (FT1), which were developed by Zadeh in 1965 and have since been effectively applied in a wide range of applications, are well known. Fuzzy type 1 (FT1) are not able to directly model such uncertainties because their membership functions have two-dimensional membership functions [21]–[22]. Such uncertainties may be managed by the interval type 2 fuzzy sets (IT2-FSs), leading to improved control performance. T2-FSs have three-dimensional membership functions while T1-FSs only have two dimensions. Thus, the newly introduced third dimension of T2-FSs offers extra degrees of freedom that can be used to directly model and control uncertainty [31]. Figure 8(a). The degree of membership in a type 2 fuzzy set is inherently fuzzy, and it is represented by what is typically referred to as a secondary MF, as shown in Figure 8(b). An IT2-FSs as depicted in Figure 8(c) is obtained if the secondary MF is at its maximum value of 1 at every point. In Figure 8(a), the secondary MF in T1-FS only has one value that corresponds to the primary membership value at which the secondary grade is equal to 1. So, for any x value in T1-FSs, there is no uncertainty about the primary membership value. Generally, the triangular secondary MF is able to simulate the uncertainty for the T2-FS depicted in Figure 8(b). Each point in the interval [a, b] has an associated secondary membership of 1, and this range serves as the primary MF for the IT2-FS shown in Figure 8(c) [12]–[13]. The IT2-FS secondary MF thus has the highest level of uncertainty. Interval type 2 fuzzy logic control (IT2FLC), which uses the same linguistic label as fuzzy type 1, is a type of fuzzy logic control (FT1). Figure 9 demonstrates the block diagram self-tuning SNPID based on the fuzzy type 2.
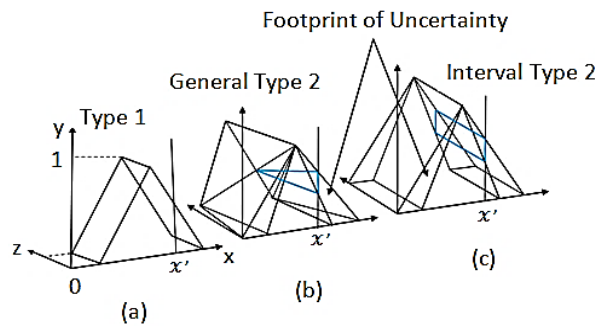

Figure 8. Illustrates several of the three kinds of fuzzy sets (a) type 1, (2) general type 2 and (c) interval type 2
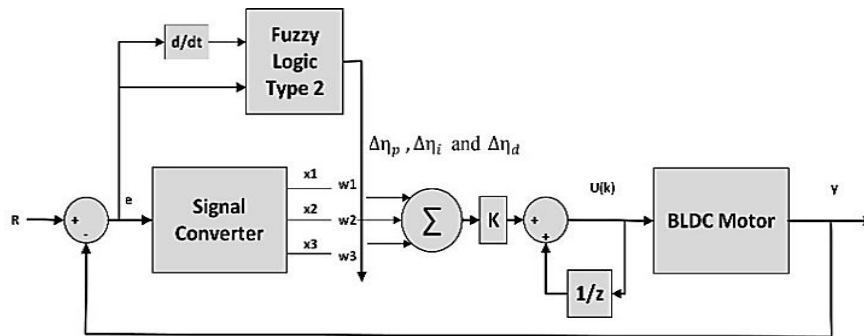

Figure 9. Fuzzy type 2 logic systems (FT2SNPID)

Interval type 2 fuzzy (IT2F), denoted $\widetilde{B}$, is described by a Type-2 MF. $\mu\widetilde{B} = (f\ c)$, where $f \in X$ and $d \in w_x \subseteq [0,1]$ i.e;

$$\widetilde{B} = \{ \left((f,c), \mu_{\tilde{A}}(f,d) \right) \Big| \ \forall f \in X, \forall d \in w_x \subseteq [0,1] \} \tag{13}$$

Where $\iint$ indicates that the union is generally admissible. f and c. For discrete universes of discourse, $\int$ is exchanged by $\sum$.

When all $\mu_{\widetilde{B}}(f,c) = 1$ then $\widetilde{B}$ is an interval type 2 FS (IT2 FS). Despite the fact that the general type 2 fuzzy set's third dimension is no longer necessary because it doesn't transmit any new information about the Interval type 2 Fuzzy (IT2F), [23] It is still possible to describe the interval type 2 fuzzy (IT2F) as a specific case of the general type 2 fuzzy.

$$\widetilde{B} = \int_{f \in X} \int_{d \in w_x} \frac{1}{(f,c)} J_x \subseteq [\,0,1] \tag{14}$$

$$\widetilde{B} = \int_{f \in D_x} \int_{d \in w_x \subseteq [0,1]} \frac{1}{(b,c)} = \int_{\in D_x} \left[\int_{d \in w_x \subseteq [0,1]} \frac{1}{c}\right]/x \tag{15}$$

Where f, called the primary factor has a domain $.D_{\tilde{x}}: f \in [0,1]$, called the secondary variable, has domain $w_x \subseteq [0,1]$ at each $f \in D_{\tilde{x}}$; w_x is also called the primary membership of f and the amplitude of $\mu_{\tilde{x}}(f,c)$, called a second grade of $\widetilde{B}$, equals 1 for $\forall f \in D_{\tilde{x}}$ and for $\forall c \in w_x \subseteq [0,1]$. The Foot of uncertainty (FOU) was bound by the upper membership function (UMF) and lower membership function (LMF) of A, as shown in Figure 10.

The UMF of $\widetilde{B}$ is the upper bound of the FOU $(\widetilde{B})$ and is denoted by the symbols $\overline{\mu}_{\tilde{b}}(f)\forall\, f \in X$, while the LMF is the lower bound of the FOU $(\widetilde{B})$ and is also denoted by the symbols $\underline{\mu}_{\tilde{b}}(f)\forall\, f \in X$ The UMF and LMF are described as (16) and (17) [24], [25]:

$$\overline{\mu}_{\tilde{x}}(f) = \overline{FOU(\widetilde{B})}\forall f \in X \tag{16}$$

$$\underline{\mu}_{\tilde{x}}(f) = \underline{FOU(\widetilde{B})}\forall\, f \in X \tag{17}$$

The calculations for IT2-FLC's fuzzification and inference were provided and described in [26].

There are two different forms of fuzzifications: the Singleton fuzzification, which is illustrated in Figure 11 [5], has a single firing input. A non-singleton firing input is used in the second type of fuzzification, as seen in Figure 11.
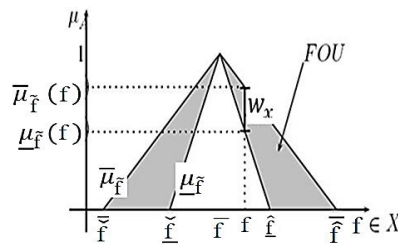

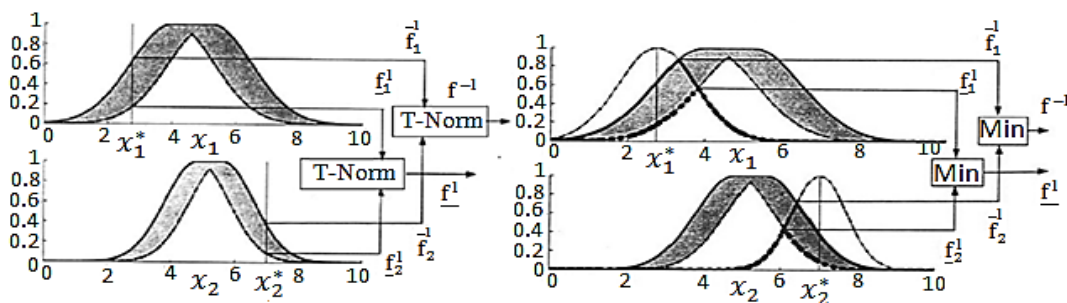Figure 10. FOU, UMF, and LMF for an Interval type 2 fuzzy set $\widetilde{B}$

Figure 11. Singleton fuzzification with minimum or product T-norm and non-singleton fuzzification with minimum T-Norm

This approach uses type-reduction to change an IT2-FLC into a T1- FLC. The inference system in Figure 12 uses a fuzzy reasoning method to produce a fuzzy output [5]. Knowledge base: contains a set of fuzzy rules, and membership functions set known as the database. A type reducer is used to transform a type 2 fuzzy set into a type 1 fuzzy set. To change a fuzzy (crisp) control action into a non-fuzzy (crisp) control action is to defuzzification it. Type reduction can be done in a variety of ways. In this study, the type reduction known as "center-of-sets" is used. This approach's computations were performed and are available in [24]. It has also been determined how to defuzzification a type-reduced set so that it produces an IT2-

FLS's clean output. Both e(t) and e(t) can be adjusted between [-5,5], while the output membership Function can be scaled between [0,10]. Figures 13 and 14 show the membership functions of the inputs and outputs of the IT2-FLC.

3.4. The COVID-19 optimization algorithm

The COVID-19 optimization technique algorithm, with its three major processes (infected individuals, intensification, and modernizing populations), is used to find the best values for the four constraints that are critical in the developing a SNPID control: K (neuron proportion factor), η_p, η_i and η_d. (Learning speed bounds). For this reason, the following multi-objective function was used in (20).
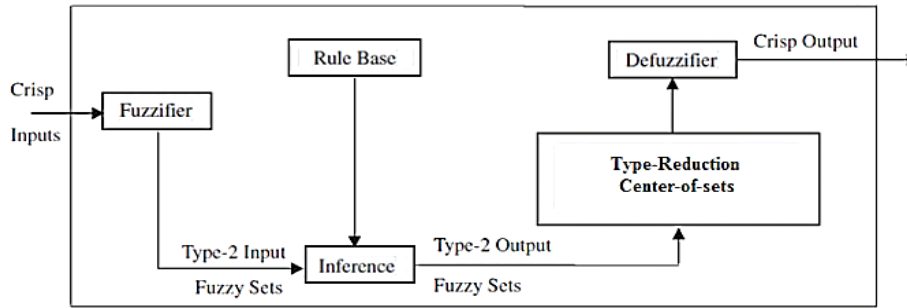

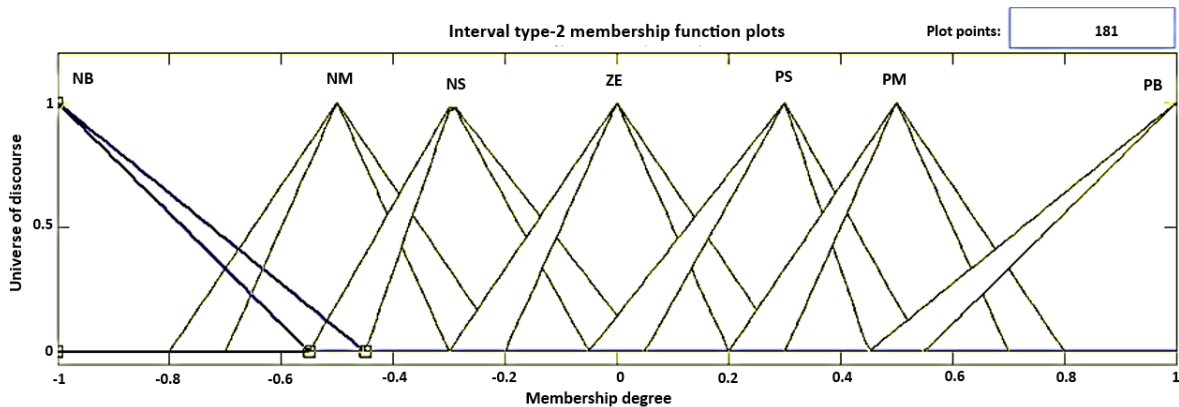Figure 12. Structure of the interval type-2 fuzzy controller

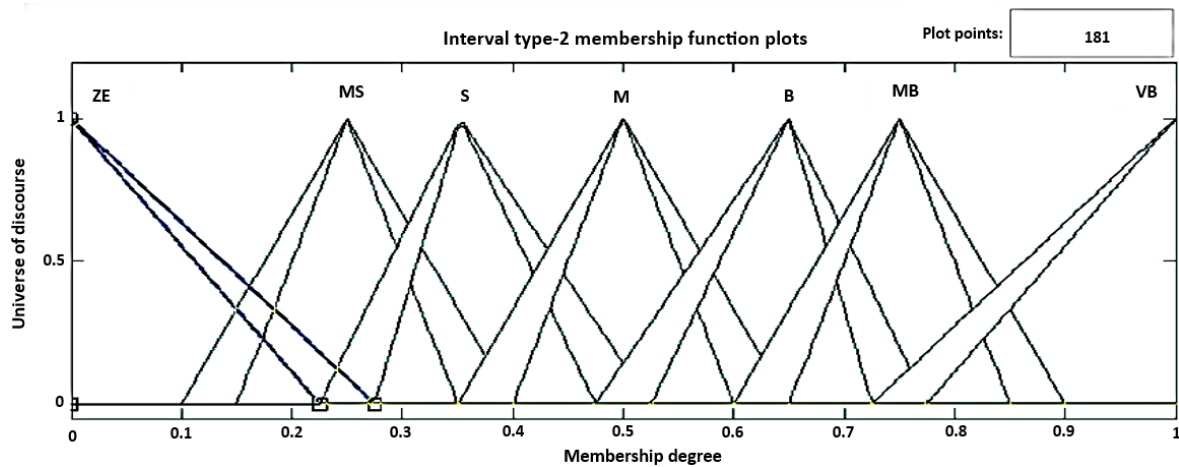Figure 13. Memberships function of inputs (e, Δe) of the IT2 FLC

Figure 14. Memberships functions of outputs ($\Delta\eta_p$, $\Delta\eta_i$ and $\Delta\eta_d$) of the IT2 FLC

The organization of optimization steps, the first stage inspects the likelihood of infection (If $\emptyset_t = 0$ then the type of distribution is $\epsilon_R = (0 \ to \ 0.5)$). If $\emptyset_t = 1$ then the type of distribution $\epsilon_{RR} = (0.5 \ to \ 1)$. The second stage, the zero diseased patient If $\emptyset_t = 0$ will convert as (17) and (18).

$$X_{F0} = R_X + (U_X - R_X)\epsilon_R \tag{17}$$

If zero diseased patient If $\emptyset_t = 1$

$$X_{F0} = R_X + (U_X - R_X)\epsilon_{RR} \tag{18}$$

The third stage explores if $H_t > P_{DIE}$ then this patient is dead and generates a newly infected patient. In case of $H_t < \emptyset_{DIE}$ then the newly infected patient will be as (19).

$$X_{new} = X_{old} \pm X_{old} \begin{bmatrix} H_1 \ D_R \\ (0.5H_2 + 0.5H_3)D_R \\ H_4 \ D_R \end{bmatrix} \tag{19}$$

The performance will be investigated according to the objective function in equation. The poor performance specifies the infected population, which has the possibility to die. While the good performance indicates the recovered population from corona antivirus.

$$H_t = (H_1 + H_2 + H_3 + H)/4 \tag{20}$$

$$H_1 = \frac{|t_r - t_{rd}|}{t_{rd}} \tag{21}$$

$$H_2 = \frac{|t_s - t_{sd}|}{t_{sd}} \tag{22}$$

$$H_3 = \frac{|e_{ss} - e_{ssd}|}{e_{ssd}} \tag{23}$$

$$H_4 = \frac{|OS - OS_d|}{OS_d} \tag{24}$$

Where (t_{rd}) is the preferred rise-time and (t_r) is the actual rise-time, (OS_d) is the wanted maximum overshoot and (OS) is the measured overshoot, (t_{sd}) is the chosen settling-time and (t_s) is the formative settling-time, and (e_{ssd}) is the favorite steady-state error and (e_{ss}) is the valued steady-state error [20].

It is clear that the cost function uses four sub-cost functions to try to satisfy the designer's objectives. Improving the rise-time of the entire drive electric system is the first sub-objective function. Trying to reduce settling time is the second sub-cost function. The steady-state error is measured by the third sub-objective function. The required overshoot is inspected by the fourth sub-objective function. The optimization will be stopped if ($X_{new} = X_{old}$) where the newly diseased populations cannot pollute new individuals. If the number of iterations ended before this previous condition. The COVID-19 optimization algorithm cannot give the optimal solution. Therefore, to obtain the optimal parameters of The SNPID controller must be $X_{new} = X_{old}$ to surety the global solution. Table 5 exhibits the used COVID-19 optimization algorithm constraints through offline optimization.

Table 5. The COVID-19 optimization algorithm parameters

No.	COVID-19 Parameter	Symbol	Value
1	Probability of death	$\emptyset_{DIE}$	ranges from 0 to 1
2	Death rate	D_R	ranges from 0 to 1
3	Distribution rate	ϵ_R	ranges from 0 to 0.5
4	Super spreading rate	ϵ_{RR}	ranges from 0.5 to 1
5	Probability of travel	$\emptyset_t$	binary value 0 or 1

4. RESULTS AND DISCUSSIONS

The results of control approaches applied to a BLDC motor drive system are shown in this section. The investigated model of BLDC motor in two cases linear and nonlinear will be exposed to sudden changes in load and operating speed during the simulation time to test the performance of each control technique. Case 1: The variable load torque disturbance is represented by no load from zero to 0.06 sec, load increase from 0.06 to 0.1 sec, and no load from 0.1 to 2 sec (nonlinear model). The system response controlled by the self-tune type 2 SNPID controller is shown in Figure 15. The self-tune type 2 SNPID controller clearly

overcomes these variances and provides good responsiveness with a short settling time. While the Self-tune type 1 SNPID controller has a huge undershoot and a longer settling time, it has a large undershoot. The self-tune type 2 SNPID controller controllers have a satisfactory control input.
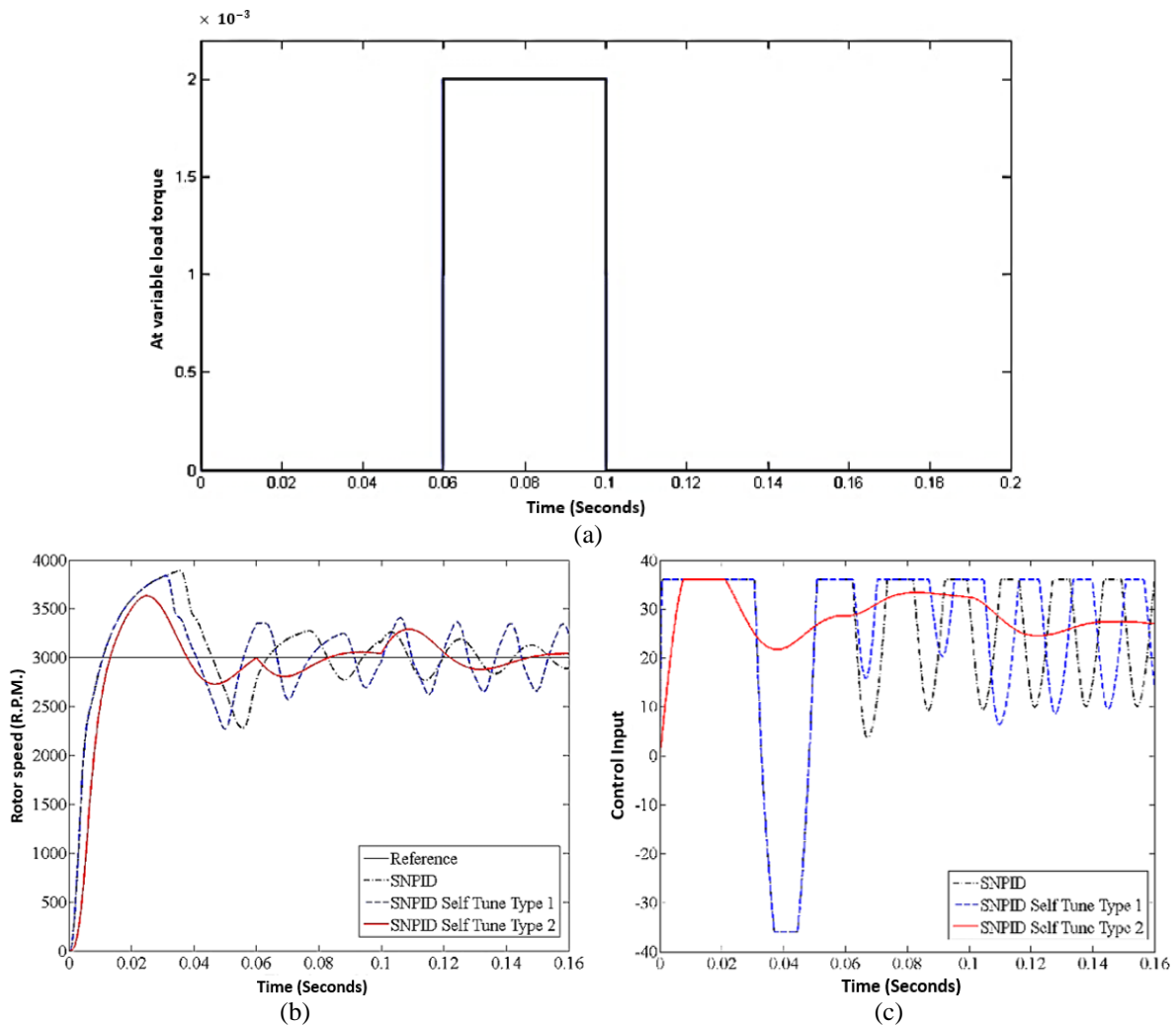

Figure 15. System dynamic responses with reference tracking case 1, (a) variable load torque disturbance, (b) rotor speed response, and (c) control input response

Case 2: The torque disturbance caused by a variable load is shown. There is no load from 0 to 0.06 seconds, the load is reduced from 0.06 to 0.1 seconds, and there is no load from 0.1 to 2 seconds (Nonlinear model). The system responses of the self-tune type 1 SNPID controller and the self-tune type 2 SNPID controller clearly seen overcome these variations and gives good response with a small settling time, as shown in Figure 16 overcomes these variations and gives better response with a small settling time, thus indicating the effectiveness of the self-tune type 2 SNPID controller over the other structure of the self-tune type 1 SNPID controller.

Several tests cannot be performed using the nonlinear model of the BLDC motor drive system. So, the following test will be executed using the linear model of BLDC motor Figure 17 to investigate the performance using the proposed control techniques. Dynamic systems usually have the characteristics of inherent nonlinearities and uncertain parameters with different disturbances. The Type 1 fuzzy controllers do not provide good performance and will be incapable of capturing all design objectives and specifications for linguistic uncertainties and nonlinearity effects under system disturbances. Thus, most research focus on type 1 fuzzy self-tuning (T1FST). It has been noted that the T1FST might not be able to handle the levels of uncertainties. The iterative type 2 fuzzy sets (IT2-FSs) might be able to handle such uncertainties and produce a better control performance at reference speed 3000 RPM.

(a)

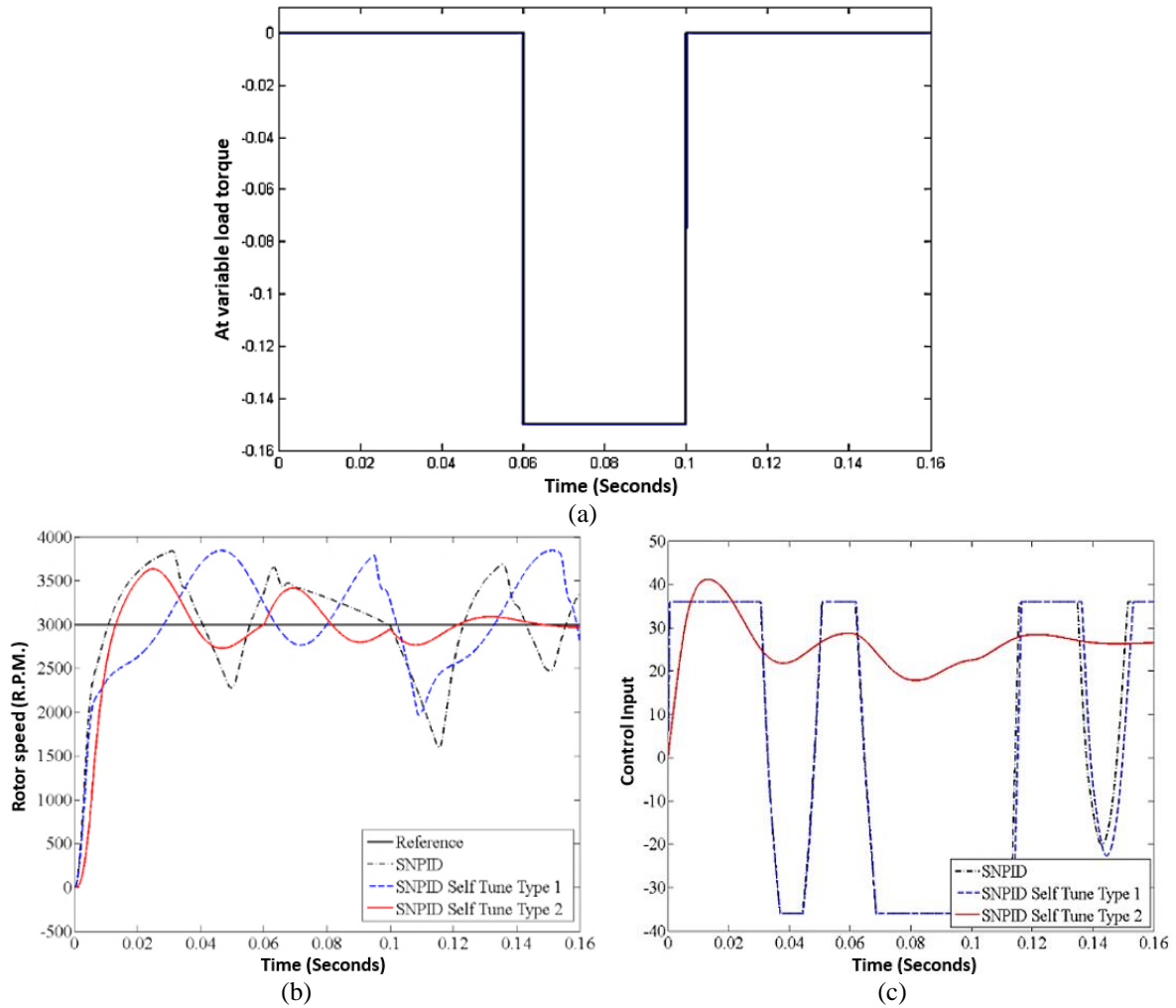(b)   (c)

Figure 16. System dynamic responses with reference tracking case 2, (a) variable load torque disturbance, (b) rotor speed response, and (c) control input response
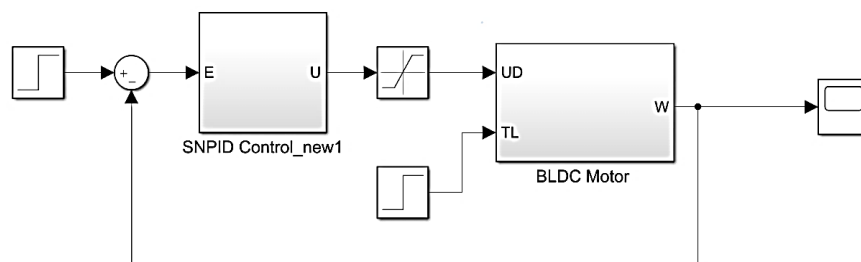

Figure 17. Linear system of BLDC motor

Case 3: At no load. In order to compare between the self-tune type 2 SNPID controller and the self-tune type 1 SNPID controller at load disturbance 0.5 % decreased is applied to the BLDC. The time response of the rotor. Speed (R.P.M) and the control input are displayed in Figure 18. It is seen that when the self-tune type 2 SNPID controller is used, the damping of the system frequency is improved significantly and settles to the nominal value quickly. In addition, it is clear that the self-tune type 2 SNPID controller responds a lot better than the self-tune type 1 SNPID controller, i.e., less overshoots oscillations with acceptable settling time than self-tune type 1 SNPID controller.

Case 4: Uncertain system parameters. The parameters Ra and La are taken into account as uncertain parameters with ± 30% of BLDC. The simulation results are shown in Figure 19 For the proposed self-tune type 2 SNPID controller, the system is shown to respond robustly to such uncertain parameters. Uncertain

System Parameters are shown in Table 6. Finally, results obtained by the self-tune type 2 SNPID controller are very encouraging in the presence of system linearity and uncertain parameters than self-tune type 1 SNPID controller.
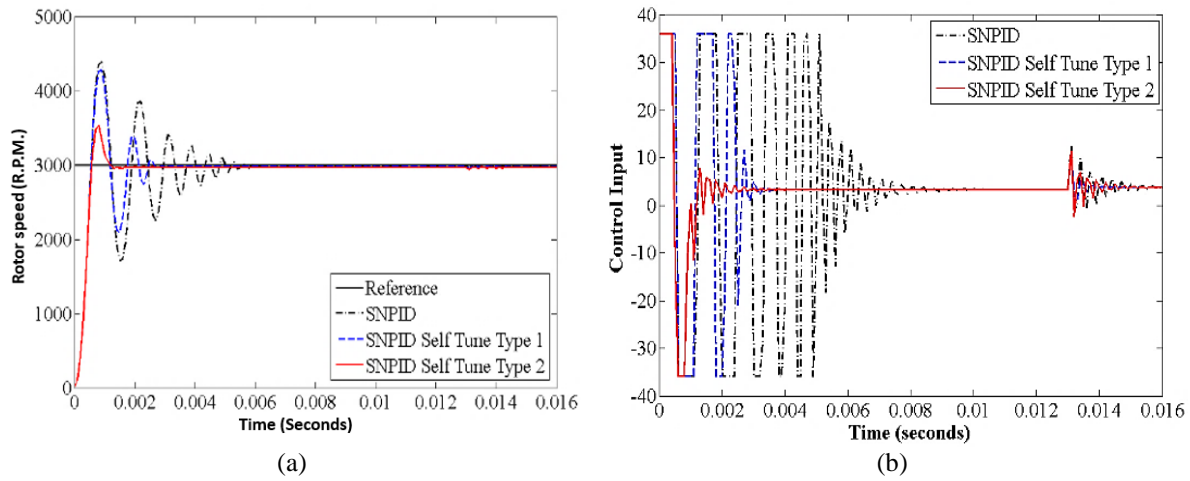

(a)   (b)

Figure 18. System dynamic responses case 3: (a) rotor speed response and (b) control input response

Table 6. Uncertain system parameters

Parameters	Normal Value	30% Increase	30 % decrease
Ra	0.5	0.65	0.3
La	6.4 e-4	8.32e-4	4.48 e-4

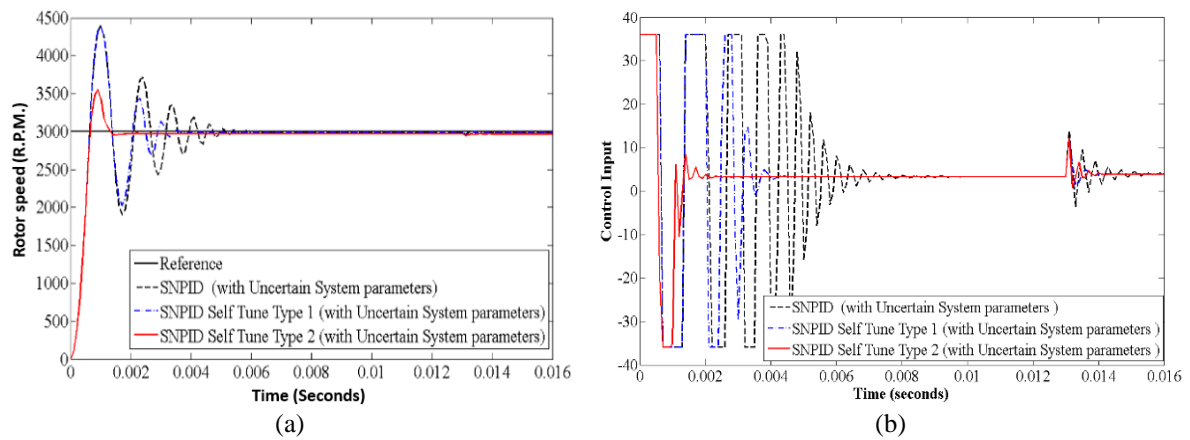(a)   (b)

Figure 19. System dynamic responses case 2: (a) rotor speed response and (b) control input response

5.   CONCLUSION

The design methods of Type 2 Self-tune fuzzy SNPID control applied to a BLDC Motor are shown in this study in order to improve performance such as decreased transient time and insensitivity to external disturbances. A comparison study was conducted between Type 2 Self-tune fuzzy SNPID, Type 1 Self-tune fuzzy SNPID, and SNPID controllers based on several tests, including parameter uncertainties and load torque variations, to investigate the proposed technique. The results have shown that the Type 2 Self-tune fuzzy SNPID, Type 1 self-tune fuzzy SNPID, and SNPID controllers are capable of providing different sufficient damping to system oscillations. Even though, the Type 2 Self-tune fuzzy. SNPID controller improves significantly the performance of the speed control of the BLDC Motor as compared to Type 1 Self-tune fuzzy SNPID and SNPID controllers. The Type 2 Self-tune fuzzy SNPID seems to be more powerful with its suitability to handle parameters uncertainty than Type 1 Self-tune fuzzy SNPID and SNPID controllers. Finally, the obtained results have demonstrated the effectiveness of the proposed Type 2 Self-

tune fuzzy SNPID controller, and the system performance was found to be satisfactory under normal and uncertain parameter cases.

REFERENCES

[1] M. A. Shamseldin, "Optimal COVID-19 based PD/PID cascaded tracking control for robot arm driven by BLDC motor," *Wseas Transactions on Systems*, vol. 20, pp. 217-227, 2021, doi: 10.37394/23202.2021.20.24.

[2] M. A. Shamseldin, "Optimal coronavirus optimization algorithm based PID controller for high performance brushless DC motor," *Algorithms*, vol. 14, no. 7, pp. 1-17, 2021, doi: 10.3390/a14070193.

[3] M. P. Maharajan and S. A. E. Xavier, "Design of speed control and reduction of torque ripple factor in BLDC motor using spider based controller," *IEEE Transactions on Power Electronics*, vol. 34, no. 8, pp. 7826-7837, 2019, doi: 10.1109/TPEL.2018.2880916.

[4] C. S. R. Reddy and M. S. Kalavathi, "Performance analysis of BLDC motor drive using new simulation model with fuzzy and ANFIS speed controllers," *Global Journals of Research in Engineering*, vol. 14, no. 4, pp. 13-20, 2014.

[5] A. Franchi and A. Mallet, "Adaptive closed-loop speed control of BLDC motors with applications to multi-rotor aerial vehicles," *IEEE International Conference on Robotics and Automation*, 2017, pp. 5203-5208, doi: 10.1109/ICRA.2017.7989610.

[6] M. Ramasamy, R. Somasundram and A. Ramasamy, "dSPACE real time implementation of fuzzy PID position controller for vertical rotating single link arm robot using four-quadrant BLDC drive," vol. 39, no. 3, pp. 301-311, 2017, doi: 10.4025/actascitechnol.v39i3.28416.

[7] S. Wen, T. Wang, Z. Ma and X. Li, "Dynamics modeling and fuzzy PD control of humanoid arm," *36th Chinese Control Conference (CCC)*, 2017, pp. 616-621, doi: 10.23919/ChiCC.2017.8027410.

[8] P. Govindan, "Evolutionary algorithms-based tuning of PID controller for an AVR system," *International Journal of Electrical and Computer Engineering*, vol. 10, no. 3, pp. 3047-3056, 2020, doi: 10.11591/ijece.v10i3.pp3047-3056.

[9] P. Kumar, M. Gupta, and V. Kunar, "Multi-objective particle swarm optimization of WEDM process parameters for inconel 825," *Journal of Computational & Applied Research in Mechanical Engineering*, vol. 10, no. 2, pp. 291-309, 2019, doi: 10.22061/jcarme.2021.1546.

[10] Z.J. Guo and X.Y. Kang, "Modeling and analysis of vehicle with wind-solar photovoltaic hybrid generating system," *4th International Conference on Sustainable Energy and Environmental Engineering*, 2016, pp. 566-570, doi: 10.2991/icseee-15.2016.95.

[11] N. A. Elkhateeb and R. I. Badr, "Novel PID tracking controller for 2DOF robotic manipulator system based on artificial bee colony algorithm," *Electrical, Control and Communication Engineering*, vol. 13, no. 1, pp. 55-62, 2017, doi: 10.1515/ecce-2017-0008.

[12] S. A. Deraz, "Genetic tuned PID controller based speed control of DC motor drive," *International Journal of Engineering Trends and Technology*, vol. 17, no. 2, pp. 88-93, 2014, doi: 10.14445/22315381/IJETT-V17P219.

[13] C. Sun, G. Gong, F. Wang, H. Yang and X. Ouyang, "Single neuron adaptive PID control for hydro-viscous drive clutch," *12th IEEE/ASME International Conference on Mechatronic and Embedded Systems and Applications (MESA)*, 2016, pp. 1-4, doi: 10.1109/MESA.2016.7587118.

[14] F. N. M. Carlos, B. M. Fotso, R. C. Talawo, and M. Fogue, "Aerodynamic analysis of an electric vehicle equipped with horizontal axis savonius wind turbines," *International Journal of Recent Trends in Engineering & Research*, vol. 5, no. 6, pp. 17-26, 2019, doi: 10.23883/ijrter.2019.5057.lkaxl.

[15] M. A. A. Ghany, M. A. Shamseldin, and A. M. A. Ghany, "A novel fuzzy self tuning technique of single neuron PID controller for brushless DC motor," *International Journal of Power Electronics and Drive System*, vol. 8, no. 4, pp. 1705-1713, 2017, doi: 10.11591/ijpeds.v8i4.pp1705-1713.

[16] N. Nisrina, M. I. Kemal, I. A. Akbar, and T. Widianti, "The effect of genetic algorithm parameters tuning for route optimization in travelling salesman problem through general full factorial design analysis," *Evergreen*, vol. 9, no. 1, pp. 163–203, 2022, doi: 10.5109/4774233.

[17] L. Wang, B. Chen and H. Z. Yang, "Single neuron PID control of aircraft deicing fluids rapid heating system," *Journal of Networks*, vol. 8, no. 2, pp. 405-412, 2013, doi: 10.4304/jnw.8.2.405-412.

[18] B. Kusumoputro and M. Rif'an, "Performance characteristics of an improved single neuron PID controller using additional error of an inversed control signal," *World Congress on Industrial Control Systems Security*, 2015, pp. 58-62, doi: 10.1109/WCICSS.2015.7420324.

[19] W. Zhao and X. Ren, "Neural network-based tracking and synchronization control for nonlinear multi-motor driving servomechanism," *35th Chinese Control Conference (CCC)*, 2016, pp. 3525-3530, doi: 10.1109/ChiCC.2016.7553901.

[20] A. Karuppannan and M. Muthusamy, "Wavelet neural learning-based type-2 fuzzy PID controller for speed regulation in BLDC motor," *Neural Computing and Applications*, vol. 33, no. 20, pp. 13481-13503, 2021, doi: 10.1007/s00521-021-05971-2.

[21] Y. Zhu, M. Feng, X. Wang and X. Xu, "Research on intelligent vehicle autonomous overtaking based on single neuron PID control," *IEEE 2nd International Conference on Cloud Computing and Intelligence Systems*, 2012, pp. 1192-1195, doi: 10.1109/CCIS.2012.6664572.

[22] M. A. A. Ghany and M. A. Shamseldin, "Parallel distribution compensation PID based on Takagi-Sugeno fuzzy model applied on Egyptian load frequency control," *International Journal of Electrical and Computer Engineering*, vol. 10, no. 5, pp. 5274-5287, 2020, doi: 10.11591/IJECE.V10I5.PP5274-5287.

[23] Y. Zhang, W. Wang, C. Xiang, C. Yang, H. Peng, and C. Wei, "A swarm intelligence-based predictive regenerative braking control strategy for hybrid electric vehicle," *Vehicle System Dynamics*, vol. 60, no. 3, pp. 973-997, 2022, doi: 10.1080/00423114.2020.1845387.

[24] M. H. Falsafi, K. Alipour, and B. Tarvirdizadeh, "Fuzzy motion control for wheeled mobile robots in real-time," *Journal of Computational & Applied Research in Mechanical Engineering*, vol. 8, no. 2, pp. 133-144, 2019, doi: 10.22061/jcarme.2018.2204.1205.

[25] C.L. Xia, *Permanent magnet brushless DC motor drives and controls*, Singapore: John Wiley & Sons Singapore Pte. Ltd., 2012.

[26] M. H. B. Chaleshtari, E. Norouzi, and H. Ahmadi, "Optimizing control motion of a human arm with PSO-PID controller," *Journal of Computational & Applied Research in Mechanical Engineering*, vol. 7, no. 1, pp. 23-34, 2017, doi: 10.22061/JCARME.2017.645.

[27] Y. R. M. K. Maher M.F. Algreer, "Design fuzzy self tuning of PID controller for chopper-fed DC motor drive," *Al-Rafidain Engineering*, vol. 16, no. 2, pp. 54-66, 2008.

[28] N. R. C. Castro, L. T. Aguilar, O. Castillo and J. R. Castro, "Type-2 fuzzy load regulation of a servomechanism with backlash using only motor position measurements," *International Conference on Fuzzy Systems*, 2010, pp. 1-8, doi: 10.1109/FUZZY.2010.5584046.

[29] M. S. Sathyanarayana, "Fuzzy implementation of model reference adaptive control of Dc drives," *International Journal of Engineering Science & Advanced Technology*, vol. 2, no. 3, pp. 605-611, 2012.

[30] T. Kumbasar and H. Hagras, "Interval type-2 fuzzy pid controllers," *Springer Handbook of Computational Intelligence*, pp. 285-294, 2015, doi: 10.1007/978-3-662-43505-3.

[31] F. F. Jaber, D. K. Shary, and H. Alrudainy, "Motion control of linear induction motor using self-recurrent wavelet neural network trained by model predictive controller," *International Journal of Power Electronics and Drive Systems*, vol. 13, no. 2, pp. 792-804, 2022, doi: 10.11591/ijpeds.v13.i2.pp792-804.

[32] N. T. García, Y. A. G. Gomez, and V. H. Cespedes, "Robust control technique in power converter with linear induction motor," *International Journal of Power Electronics and Drive Systems*, vol. 13, no. 1, pp. 340-347, 2022, doi: 10.11591/ijpeds.v13.i1.pp340-347.

[33] Y. Anagreh, M. B. Fayyad, and A. Anagreh, "Particle swarm optimization based high performance four switch BLDC motor drive," *International Journal of Power Electronics and Drive Systems*, vol. 13, no. 2, pp. 825-834, 2022, doi: 10.11591/ijpeds.v13.i2.pp825-834.

[34] W. Aribowo, Supari, and B. Suprianto, "Optimization of PID parameters for controlling DC motor based on the aquila optimizer algorithm," *International Journal of Power Electronics and Drive Systems*, vol. 13, no. 1, pp. 216-222, 2022, doi: 10.11591/ijpeds.v13.i1.pp216-222.

[35] M. Al-Nasrawi, A. Al-Ghanimi, and A. A. A. Mashkor, "A tracking control design for linear motor using robust sliding mode learning control," *International Journal of Power Electronics and Drive Systems*, vol. 13, no. 2, pp. 960-968, 2022, doi: 10.11591/ijpeds.v13.i2.pp960-968.

[36] D. Potnuru, T. S. L. V. Ayyarao, L. V. S. Kumar, Y. V. P. Kumar, D. J. Pradeep, and C. P. Reddy, "Salp swarm algorithm based optimal speed control for electric vehicles," *International Journal of Engineering Trends and Technology*, vol. 13, no. 2, pp. 755-763, 2022, doi: 10.11591/ijpeds.v13.i2.pp755-763.

[37] C. T. Yaw, S. Y. Wong, and K. S. Yap, "An ELM-based single input rule module and its application in power generation," *International Journal of Power Electronics and Drive Systems*, vol. 11, no. 1. pp. 359-366, 2020, doi: 10.11591/ijpeds.v11.i1.pp359-366.

[38] G. A. Salman, A. S. Jafar, and A. I. Ismael, "Application of artificial intelligence techniques for LFC and AVR systems using PID controller," *International Journal of Power Electronics and Drive Systems*, vol. 10, no. 3. pp. 1694-1704, 2019, doi: 10.11591/ijpeds.v10.i3.1694-1704.

[39] K. Aseem and S. S. Kumar, "Closed loop control of dc-dc converters using pid and fopid controllers," *International Journal of Power Electronics and Drive Systems*, vol. 11, no. 3. pp. 1323-1332, 2020, doi: 10.11591/ijpeds.v11.i3.pp1323-1332.

[40] B. Azhari, P. Irasari, and P. Widianto, "Design and simulation of 5kw bldc motor with half-buried permanent magnets using an existing stator body," *International Journal of Power Electronics and Drive Systems*, vol. 12, no. 4. pp. 2030-2043, 2021, doi: 10.11591/ijpeds.v12.i3.pp2030-2043.

[41] S. S. Sami, Z. A. Obaid, M. T. Muhssin, and A. N. Hussain, "Detailed modelling and simulation of different dc motor types for research and educational purposes," *International Journal of Power Electronics and Drive Systems*, vol. 12, no. 2. pp. 703-714, 2021, doi: 10.11591/ijpeds.v12.i2.pp703-714.

[42] N. Farah, M. H. N. Talib, Z. Ibrahim, J. M. Lazi, and M. Azri, "Self-tuning fuzzy logic controller based on Takagi-Sugeno Applied to induction motor drives," *International Journal of Power Electronics and Drive System*, vol. 9, no. 4, pp. 1967-1975, 2018, doi: 10.11591/ijpeds.v9.i4.pp1967-1975.

BIOGRAPHIES OF AUTHORS

Mohamed A. Abdel Ghany was born in Cairo 22th July 1988. He received his B. Sc from Higher Technological Institute (Tenth of Ramadan City) 2011, Diploma and M.Sc. in Automatic Control (2012 to 2014) from, Helwan University, Cairo, Egypt. From 20/6/2015 to 2018, he worked as an Assistant Lecturer at Faculty of Computer science Nahda University, Bani Sweif City. He obtained his Ph. D in Automatic Control branch in Faculty of Engineering, Helwan University, Egypt. Now, he worked as an assistant professor at department of Electrical Engineering, Faculty of Engineering October 6 University, Egypt. He can be contacted at email: m.a.abdelghany.eng@o6u.edu.eg.

Mohamed A. Shamseldin received M.Sc. degree in system automation and engineering management and the Ph.D. degree in mechatronics engineering both from the Helwan University, Cairo, Egypt, in 2016 and 2020, respectively. In 2018, he was a Lecturer with the Faculty of Engineering, University of Central Lancashire, UK. Currently, he is an assistant Professor with the faculty of engineering and technology of Mechatronics Engineering, Future University in Egypt, Cairo, Egypt. His research interests include electric machine drives, mechatronics, robot control, system automation, and electric vehicle. He can be contacted at email: Mohamed.abelbbar@fue.edu.eg.